npj | quantum materials

Article

Published in partnership with Nanjing University

https://doi.org/10.1038/s41535-024-00642-6

Coherent phonon and unconventional carriers in the magnetic kagome metal Fe_3Sn_2

Marcos V. Gonçalves-Faria [1,2] ✉, Alexej Pashkin[1], Qi Wang[3], Hechang C. Lei [3], Stephan Winnerl[1], Alexander A. Tsirlin [4], Manfred Helm[1,2] & Ece Uykur [1] ✉

Temperature- and fluence-dependent carrier dynamics of the magnetic kagome metal Fe_3Sn_2 were studied using the ultrafast optical pump-probe technique. Two carrier relaxation processes and a laser-induced coherent optical phonon were observed. We ascribe the shorter relaxation (~1 ps) to hot electrons transferring their energy to the crystal lattice via electron–phonon scattering. The second relaxation (~30 ps), on the other hand, cannot be explained as a conventional process, and we attributed it to the unconventional (localized) carriers in the material. The observed coherent oscillation is assigned to be a totally symmetric A_{1g} optical phonon dominated by Sn displacements out of the kagome planes and possesses a prominently large amplitude, on the order of 10^{-3}, comparable to the maximum of the reflectivity change (ΔR/R). This amplitude is similar to what has been observed for coherent phonons in charge-density-wave (CDW) systems, although no signs of such instability were hitherto reported in Fe_3Sn_2. Our results suggest an unexpected connection between Fe_3Sn_2 and kagome metals with CDW instabilities and a strong interplay between phonon and electron dynamics in this compound.

During the last years magnetic kagome metals have emerged as an interesting class of materials due to their unusual properties. In terms of electronic structure, a simple tight-binding model constructed on the kagome lattice is well known to result in dispersionless flat bands and Dirac cones[1]. Thus, unconventional (localized) carriers due to the correlation effects together with topological states are expected for these materials. Combining such features with magnetism makes magnetic kagome metals suitable to host different types of exotic phenomena, and in this regard, the family of kagome FeSn-binary compounds (FeSn, Fe_3Sn, Fe_3Sn_2) presents several promising candidates. For Fe_3Sn_2, both the linearly dispersing bands and the flat bands were previously observed experimentally[2,3], and recently it attracted great attention after discoveries of massive Dirac fermions[2], large anomalous Hall effect[4], skyrmion bubbles at room temperature[5] and tunable spin textures using an external magnetic field[6].

Fe_3Sn_2 is a layered rhombohedral material belonging to the $R\bar{3}m$ space group, with hexagonal lattice parameters $a = b = 5.3$ Å and $c = 19.8$ Å[7]. Its crystalline structure is composed of Fe_3Sn kagome bilayers, where the Fe kagome network is stabilized with Sn1 atoms and sandwiched between honeycomb Sn2 layers [Fig. 1b, c]. Furthermore, Fe_3Sn_2 presents an in-plane lattice distortion known as breathing kagome[2]. Here the length of Fe–Fe bonds varies slightly, generating triangles with two different sizes in the kagome plane, as highlighted in Fig. 1c. Regarding the magnetic structure, Fe_3Sn_2 is a ferromagnetic material with high ordering temperature, $T_C \sim 640$ K[7–9]. The magnetic moments first align in the out-of-plane direction, and by cooling the system down, the spins realign to the in-plane direction. This process happens in a broad temperature range, around 150 K, and its signatures were observed with several different experimental techniques, such as Mössbauer[9,10], neutron diffraction[7], electronic transport[11], and infrared spectroscopy[12]. This magnetic transition is also reflected in some of the optical pump-probe results in the present work, which will be discussed in more detail later.

It has been shown that the observed properties of Fe_3Sn_2 are closely related to the peculiarities of its lattice and magnetic structure[2,13]. The fingerprints of the non-trivial carrier dynamics have been identified in optical studies[12], whereas the interplay of the topological orders with magnetism and strongly correlated electrons is yet to be clarified. The

[1]Institute of Ion Beam Physics and Materials Research, Helmholtz-Zentrum Dresden-Rossendorf, 01328 Dresden, Germany. [2]Technische Universität Dresden, 01062 Dresden, Germany. [3]Department of Physics and Beijing Key Laboratory of Opto-electronic Functional Materials & Micro-Nano Devices, Renmin University of China, Beijing 100872, China. [4]Felix Bloch Institute for Solid-State Physics, Leipzig University, 04103 Leipzig, Germany. ✉e-mail: m.goncalves-faria@hzdr.de; e.uykur@hzdr.de

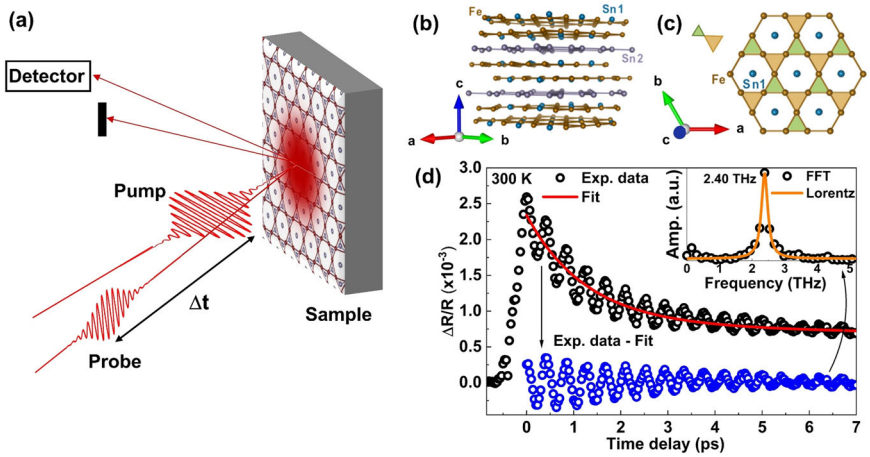

Fig. 1 | Optical pump-probe experiment on Fe_3Sn_2. **a** Basic schematic of the optical pump-probe experiment in the reflectivity configuration. **b** Crystal structure of Fe_3Sn_2, with Fe_3Sn1 kagome bilayers and honeycomb Sn2 layers. Sn1 atoms from the trigonal kagome layer and Sn2 atoms from the honeycomb lattice are distinguished using different colors to facilitate the view. **c** Fe–kagome network centered by the Sn1 atoms and the breathing kagome bonds demonstrated with triangles of different colors. **d** Optical pump–probe trace of Fe_3Sn_2 at 300 K with the fluence of 1.6 mJ cm^{-2}. Black dots are experimental data, and the red solid line is the exponential fit according to Eq. (1). Blue dots are the result of subtracting the exponential fit from the experimental data, isolating the oscillatory part of the signal. Inset shows the Fourier transform of the coherent oscillations, with a resonance frequency of about 2.40 THz, corresponding to one of the A_{1g} totally symmetric phonon modes of Fe_3Sn_2.

tunability of different contributions is highly desirable, also for possible future applications of Fe_3Sn_2.

Here, we present an ultrafast optical pump–probe spectroscopy investigation on Fe_3Sn_2, as shown schematically in Fig. 1a. This method has been extensively used to study the dynamics of non-equilibrium charge carriers and coherent phonons in solids[14–18], and it is well suited to study metallic systems[19–22], where different contributions can be identified. So far, the ultrafast dynamics of kagome metals have not been widely explored. There is one report on the magnetic compound $GdMn_6Sn_6$[23] where a low amplitude coherent phonon was observed. The charge-density-wave (CDW) compounds, on the other hand, received a bit more attention with a few reports on CsV_3Sb_5[24–26] and a recent study on ScV_6Sn_6[27], where the ultrafast response of the unusual CDW state has been probed. In this letter, we report the temperature- and fluence-dependent transient reflectivity measurements of Fe_3Sn_2. Our results reveal strong coherent phonon oscillations in Fe_3Sn_2, with intriguing similarities to the CDW case, even though no CDW has been reported in Fe_3Sn_2 as a ferromagnetic Kagome metal. Thus, indicating the electron-phonon coupling as the possible mechanism related to the unconventional carriers in kagome metals.

Results

Figure 1d presents the general behavior of our transient reflectivity measurements. Here, reflectivity change ($\Delta R/R$) is given as a function of the pump-probe time delay at 300 K with pump fluence of 1.6 mJ cm^{-2}. The best fit for all pump-probe traces was achieved with the following equation:

$$\Delta R/R = y_0 + c_1 \exp(-t/\tau_1) + c_2 \exp(-t/\tau_2), \quad (1)$$

where c_1 and c_2 are constants, y_0 is an offset parameter and τ_1 and τ_2 are relaxation times. The time scales of the relaxations are: τ_1 in the order of ~1 ps and τ_2 in the order of a few tens of picoseconds, both processes will be discussed with more detail as a function of temperature and excitation fluence. The offset term, y_0, can be understood as a much longer thermal relaxation, and due to experimental limitations, it had to be approximated as a constant. Another interesting feature is that around the first ~8 ps after pump-probe temporal overlap, the decaying signal is modulated by pronounced oscillations. This is the coherent optical phonon induced by the ultrashort pump pulse that will also be further analyzed as a function of temperature and fluence.

Relaxations

The temperature dependence of the transient reflectivity, the obtained relaxation times, and the offset constant y_0 are given in Fig. 2a–d, whereas Fig. 2e depicts c_1 and c_2, the constants representing the amplitude of the τ_1 and τ_2 according to Eq. (1), respectively. Figure 2f–j demonstrates the fluence dependence of the same parameters. We limited the time delay to 8 ps, longer time delays can be found in Supplementary Fig. 1.

Due to the metallic nature of Fe_3Sn_2[11], τ_1, and y_0 can be explained using the phenomenological two-temperature model (TTM) for metals[19,20,28], where τ_1 is the relaxation of the hot electrons, and y_0 reflects the dissipation of the residual lattice heating. As given in Fig. 2b, τ_1 is temperature independent, lying around 1.1 ps. y_0, on the other hand, increases with increasing temperature up to around 175 K, and then it saturates for higher temperatures, indicating that cooling down the sample removes the excess heat and brings the system to equilibrium faster [Fig. 2d]. The fluence dependencies of τ_1 and y_0 also corroborate this explanation, as seen in Fig. 2g and i, respectively. By simply taking into account the electron/lattice temperature and the electron–phonon coupling, the increase of τ_1 with fluence can be nicely reproduced by the TTM model [purple solid line in Fig. 2g]. A similar change has also been observed at 10 K and 170 K (see Supplementary Note 2 and Supplementary Fig. 8 for details about the TTM and the analysis for 10 K and 170 K).

Coming to the τ_2, the dynamics behind this process indicate a departure from a simple Drude metal. Considering that the spectra are dominated by the coherent phonon oscillations and the excess heat of the system generates a background, τ_2 is more reliably extracted at low temperatures, where y_0 vanishes. The τ_2 value is weakly temperature dependent [Fig. 2c] changing from 30 ps to ~25 ps with decreasing temperature. At high temperatures, we did not observe any fluence dependence [Fig. 2h]. With the decreasing temperature at lower fluences, a small decrease is present, and it goes into the saturation limit at higher pump fluences.

Previous optical studies[12] indicated that Fe_3Sn_2 is not a simple metal. Its optical conductivity shows two distinct intraband contributions. A sharp Drude contribution is accompanied by a second peak due to the localized carriers (localization peak), which is the common situation on both magnetic and nonmagnetic kagome metals[12,29–32]. Considering that the traditional metallic behavior expected for an optical pump-probe experiment is already taken into account by τ_1 and y_0, we ascribe τ_2 to the ultrafast response coming from the localized carriers. Here pumping leads to the

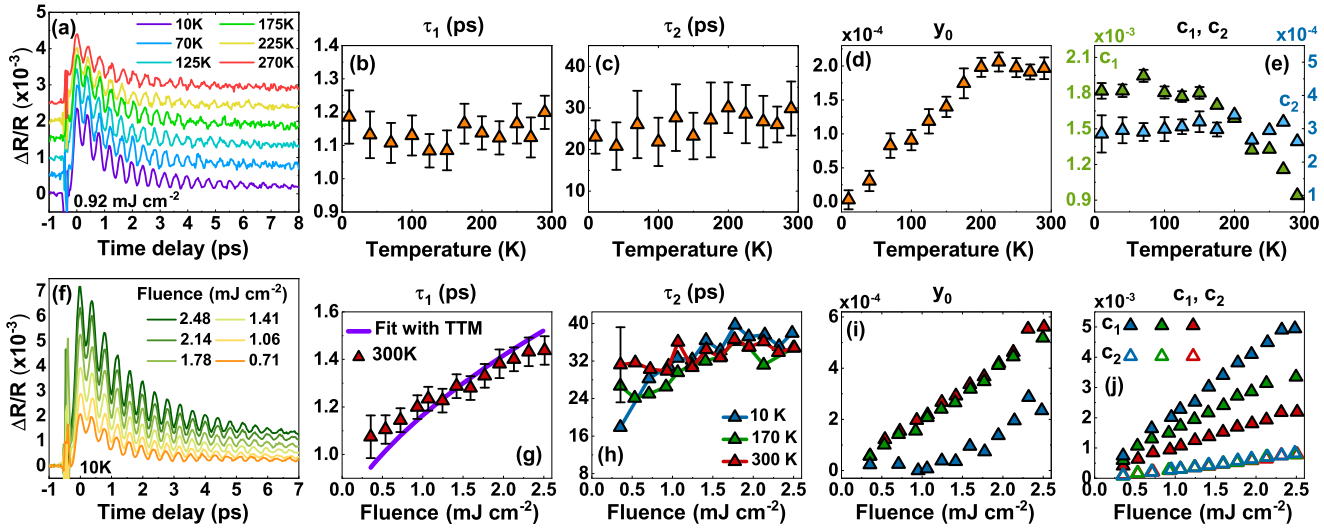

Fig. 2 | Temperature- and fluence-dependence results from the transient reflectivity experiment. a Temperature-dependent optical pump-probe traces of Fe_3Sn_2 using 0.92 mJ cm^{-2}. The curves at different temperatures are separated by a 0.5×10^{-3} offset. **b**–**e** present the Eq. (1) parameters τ_1, τ_2, y_0, c_1, and c_2, respectively. Fluence-dependent experimental data at 10 K are shown in (**f**). Panels **g**–**j** are τ_1, τ_2, y_0, c_1, and c_2 as a function of pump fluence. The purple solid line in **g** is fit for τ_1 using the two-temperature model at 300 K. Fluence dependence results for τ_1 at all temperatures are quite similar, so for better visualization, the data and the fits at 170 and 10 K were added to the Supplementary Fig. 8. Omitted error bars in panels **e**, **i** and **j** are due to the uncertainty being smaller than the actual points. In panel **h** the error bars were omitted for better visualization, only the biggest one, at 300 K and 0.35 mJ cm^{-2} is shown. In all panels, error bars represent the confidence interval of the exponential fitting procedure.

delocalization of these unconventional carriers, and we believe to be observing the time scale of the localization process. The amplitude of this process should be proportional to the spectral weight of the localization peak observed in the broadband IR spectroscopy measurements[12]. Indeed a direct comparison reveals a temperature-independent behavior for both the spectral weight of the localization peak [Fig. S5(e) of Ref. 12] and the amplitude of τ_2 [c_2 in Fig. 2e].

The temperature-driven dynamics show a different evolution of c_1 and c_2, as given in Fig. 2e. While with decreasing temperature, c_2 does not change, c_1 shows a slight increase and saturates below the spin-reorientation temperature. Here the change of the carrier density is probably not related to the change in the Fermi level with temperature, but rather with gapping of certain parts of the Fermi surface upon the reorientation of the spins. With increasing fluence, on the other hand [Fig. 2j], a linear increase is observed for both c_1 and c_2, which is consistent with the increase of photo-excited carriers at higher fluences.

Phonon mode

Now let us turn to the coherent optical phonon identified in the spectra. These laser-induced oscillations are generated by the lattice atoms vibrating in phase to each other, and measured as a periodic modulation of the optical properties[18,33,34]. In Supplementary Note 1 the details regarding data analysis for the resonance frequency and amplitude of the mode can be found. Such coherent phonon oscillations are reported for different systems in the literature[18,34–38]. However, the strength of these oscillations in the current measurements is an interesting finding. Such strong oscillations are usually observed in systems with CDW instabilities and other types of collective order as for example in the case of $K_{0.3}MoO_3$[39,40], VO_2[41] and the kagome $CsV_3Sb_{5-x}Sn_x$[42] with a coherent phonon that becomes Raman-active only through coupling to the CDW order. Fe_3Sn_2, however, is not known to host any of such instabilities. Elemental crystal systems without CDW may also present such strong features, like Bi[34,43] and Sb[18], however, in both cases, there is at least a periodic lattice modulation related to the excited mode. On the other hand, the correlated nature of the kagome metals has been identified by different means, including the observation of the aforementioned localization peak in the optical spectra. Here, the intraband carriers are damped by the back-scattering from the collective modes, which in principle, can have any bosonic excitation as the origin. Our observation of this unusual phonon coupling makes phonons a plausible candidate for this collective mode.

Figure 3a–c depicts the temperature dependence of the obtained phonon parameters, namely the resonance frequency, amplitude, and width. Its frequency, retrieved using a Fourier transform, was found to be around 2.40–2.50 THz, which corresponds to an A_{1g} totally symmetric mode[44]. As also shown in Fig. 3, this is primarily an Sn mode where the Sn1 atoms from the center of the hexagons in the kagome plane move only in the out-of-plane direction. Thus, it does not affect the Kagome network significantly. The mode is dependent on both temperature and magnetic structure, presenting a clear phonon softening with increasing temperature and anomalies on its amplitude and peak width around the spin reorientation temperature range (~150 K). The shaded area in Fig. 3a–c highlights this temperature range where the magnetic transition takes place. While the spins realign from out-of-plane to in-plane the phonon amplitude shows a plateau-like behavior. The phonon softening and the increase of the amplitude of the phonon oscillations have also been observed with increasing fluence, as shown in Supplementary Fig. 5.

Phonon softening with temperature and fluence is often attributed to anharmonic terms in the vibrational potential energy[45,46]. However, other signatures of these anharmonic effects are not observed in our data. For instance, the amplitude does not follow the expected increasing behavior with decreasing temperature and shows a plateau around the spin reorientation temperature. Furthermore, the width does not show a monotonous decrease with decreasing temperature. In fact, it hardly changes. Other evidence against the anharmonic phonon softening is that the decay rate of the phonon does not change significantly with temperature (see Supplementary Fig. 3). To be sure about the behavior of all the phonon parameters, we measured the temperature dependence more than once. Figure 3a–c presents an average from the different data sets.

Along with the evidence against the anharmonic phonon coupling, the absence of E_g phonon modes, the cosine-like character of the oscillations, shown in Supplementary Fig. 4, and the large amplitude of the oscillations when compared to the non-oscillatory decaying signal (also increasing linearly with fluence), are strong indications of displacive excitation of coherent phonons (DECP) as the mechanism behind this coherent phonon

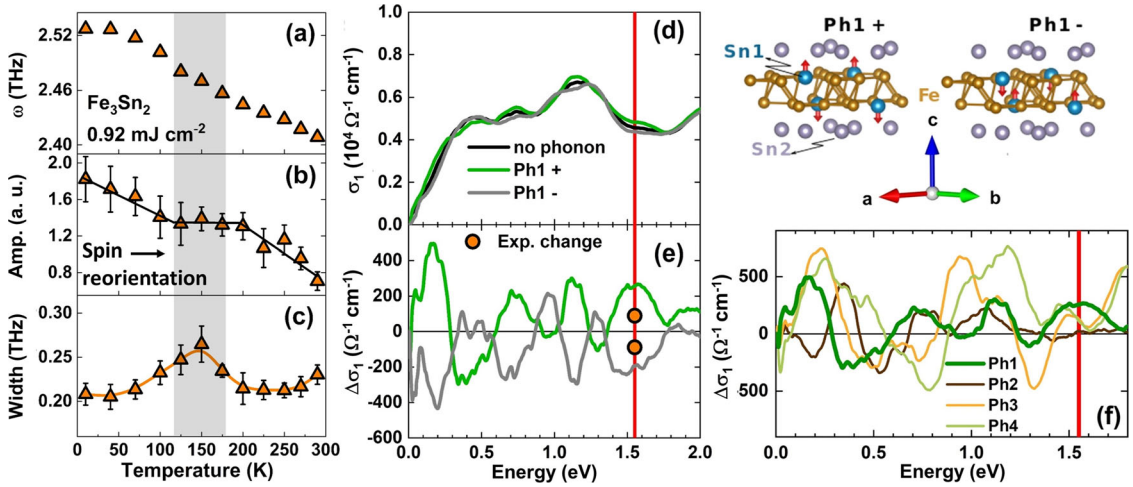

Fig. 3 | Coherent phonon evolution with temperature and comparison with DFT optical conductivity calculations. Temperature dependence of **a** frequency, **b** amplitude, and **c** width of the A_{1g} phonon mode in Fe_3Sn_2. The shaded area in **a**–**c** is to highlight the temperature range where the system goes through a spin reorientation. The lines in **b** are guides to the eyes. **d** Presents the calculated optical conductivtiy via DFT for the nominal Fe_3Sn_2 along with the distorted structure under A_{1g} phonon mode. **e** Depicts the change in optical conductivity under the influence of the phonon mode. The orange circles are the change of the optical conductivity estimated by changing the experimental reflectivity[12] by 10^{-3}. The red line in **d** and **e** is the pump–probe frequency of 800 nm. **f** Difference in the optical conductivity with respect to the nominal value for all the A_{1g} modes, with Ph1 being the one measured in our experiments. Bilayer kagome structure has been given on top of **f** with the representation of the A_{1g} phonon mode demonstrated with the red arrows. Error bars in panel **a** are smaller then the points, therefore, they were omitted. For **b** and **c**, the error bars show the standard deviation considering all the temperature-dependent measurements.

generation[47]. This indicates a strong electron–phonon coupling in Fe_3Sn_2 in both low and room-temperature regimes, as DECP depends exclusively on this coupling to induce coherent oscillations. The maximum of the non-oscillatory exponential decay increases with fluence, indicating a larger photo-excited carriers density at higher fluences, and then a considerable electronic softening of the lattice is expected[37,48]. As a consequence, the reduction of the restoring force for the A_{1g} lattice displacement appears naturally with the excitation of a larger number of electrons. Thus, this phenomenon can be understood as solely an electronic softening of the crystal lattice.

Discussion

Such a strong phonon coupling suggests some sort of an incipient lattice distortion in Fe_3Sn_2. At first glance, the breathing kagome distortion [Fig. 1(c)], where the successive Fe-bonds in kagome network are slightly different, is a reasonable cause. On the other hand, in this case, it is expected that the breathing E_g mode, which directly affects the kagome network, would be the phonon that modulates reflectivity. Considering that the observed A_{1g} mode does not affect this breathing kagome structure, this assumption seems to be unlikely. This, therefore, distinguishes Fe_3Sn_2 from systems like Bi and Sb, where as discussed earlier, the strong reflectivity modulation can be understood solely in the context of a periodic lattice distortion, raising again the question of why such high coherent phonon amplitude is present in Fe_3Sn_2.

Another possibility why Fe_3Sn_2 is special lies in the proclivity of kagome metals for CDW instabilities that have been revealed not only in nonmagnetic compounds like AV_3Sb_5 and ScV_6Sn_6[24,25,49,50], but also in the magnetic kagome metal FeGe[51]. Our data support growing evidence that even in the absence of a CDW transition, charge carriers in kagome metals can be strongly coupled to specific phonons that, in turn, have a crucial effect on their dynamics.

Finally, we use density-functional-theory (DFT) to elucidate the effect of the A_{1g} phonon mode on the optical conductivity, details of the calculations are given in Supplementary Note 3. We have introduced the atomic displacements due to the phonon mode, as demonstrated in Fig. 3, and calculated the optical conductivity as given in Fig. 3d. The displacement amplitude is taken as 0.1 Å, which is consistent with the estimated atomic displacement (see Supplementary Fig. 10). To demonstrate changes in the optical conductivity, and ensuing changes in the reflectivity, we have plotted in Fig. 3e the difference in optical conductivity with respect to the undistorted structure. The results suggest that at 800 nm [red line in Fig. 3e], the observed 2.5 THz phonon mode has a strong impact on the optical conductivity and can clearly be the reason behind the observed 10^{-3} change in the reflectivity (the orange circles are the estimates over the experimental reflectivity spectra). The distortion of the structure in two opposite directions nicely leads to a symmetric change of the optical conductivity. For comparison, changes in the optical conductivity induced by all four A_{1g} modes have also been calculated, as shown in Fig. 3f (details about the lattice displacement of the three other modes are presented in Supplementary Fig. 9). Such results suggest that at 800 nm, the most prominent change is due to the observed 2.5 THz A_{1g} mode, and other modes do not alter the optical conductivity significantly. These calculations may also explain why we could measure only a single phonon mode as a reflectivity modulation while the other totally symmetric A_{1g} modes were not observed.

In summary, photo-induced changes in reflectivity of the kagome metal Fe_3Sn_2 reveal the dynamics of carriers and coherent optical phonons rendering Fe_3Sn_2 different than conventional metals. We detect three time scales. Two of them, the faster and slower ones, are clearly related to the highly metallic nature of the material and can be well explained using the two-temperature model for conventional metals. Regarding the medium time scale, on the other hand, we believe to be probing the localization time of the unconventional carriers that get delocalized due to laser pumping. Their distinct relaxation time and coupling to short optical pulses allow an independent probe of Drude and localized carriers, as well as the control of localization using ultrafast optical probes. Additionally, strong coherent phonon oscillations have been observed, indicating a strong electron-phonon coupling in Fe_3Sn_2 even at room temperature. The nature of this phonon mode is attributed to the electronic softening of the crystal lattice due to the large photo-induced carrier density. The spin reorientation of Fe_3Sn_2 around 150 K does not seem to have a significant effect on the dynamics of charge carriers, although it manifests itself in the temperature dependence of the coherent phonon. In conclusion, our study demonstrates the salient role of phonon dynamics and electron-phonon coupling even in those kagome metals where no CDW instabilities occur.

Methods

Sample details

Single crystals of Fe_3Sn_2 were grown using the self-flux method as described elsewhere[11]. The (001)-plane with lateral dimensions of 1000 μm × 800 μm × 200 μm is used for the optical pump–probe transient reflectivity measurements. We used the same as-grow sample as in our previous infrared spectroscopy study[12].

Transient reflectivity measurements and data analysis

Temperature- and fluence-dependent optical pump-probe experiments were performed in the reflection geometry. For both pump and probe, we used 60 fs long laser pulses, centered at 800 nm and generated by a Ti:sapphire laser amplifier with 250 kHz repetition rate. The probe spot on the sample surface was around 25 μm (FWHM), while the pump was 35 μm (FWHM). Transient reflectivity was measured up to 150 ps delay time with 1 ps time resolution. Up to around 9 ps delay time, we increased the time resolution to 33 fs to resolve the phonon oscillations.

The overall temperature and fluence dependence of the transient reflectivity does not change drastically and can be fitted solely by employing Eq. (1). By subtracting this fitting from the experimental data, it is possible to isolate the oscillations. The fast Fourier transform (FFT) of these oscillations gives the resonance frequency of the phonon mode that couples to the electronic background. Using a Lorentzian function we fitted the FFT spectrum in order to obtain the amplitude and the width of the phonon mode, as discussed in the main text.

Density functional theory calculations

Density-functional-theory (DFT) calculations of the band structure were performed in the `Wien2K`[52,53] code using the Perdew–Burke–Ernzerhof flavor of the exchange-correlation potential[54]. We used experimental structural parameters determined by X-ray diffraction measurements. The `optic` module[55] was used for evaluating the optical conductivity. Spin-orbit coupling was included in the calculations of band structure and optical conductivity. Furthermore, ferromagnetic order was taken into account, where the spins on Fe-atoms are aligned along the in-plane direction, which eventually occurs below the spin-reorientation temperature. The DFT-obtained magnetic moment per Fe-atom was 2.18 μ_B, which is very close to the experimental values[11]. Self-consistent calculations were converged on the 24 × 24 × 24 k-mesh. Optical conductivity was calculated on the k-mesh with up to 100 × 100 × 100 points within the Brillouin zone.

The phonon calculations were performed in `VASP` using the same structural parameters and the built-in procedure with frozen atomic displacements of 0.015 Å. Magnetic moments were directed along the c-axis to avoid symmetry lowering.

Data availability

The data that support the findings of this study are available from the corresponding authors upon request.

Received: 7 November 2023; Accepted: 11 March 2024;
Published online: 21 March 2024

References

1. Kang, M. et al. Dirac fermions and flat bands in the ideal kagome metal FeSn. *Nat. Mater.* **19**, 163–169 (2020).
2. Ye, L. et al. Massive Dirac fermions in a ferromagnetic kagome metal. *Nature* **555**, 638–642 (2018).
3. Lin, Z. et al. Flatbands and emergent ferromagnetic ordering in Fe_3Sn_2 kagome lattices. *Phys. Rev. Lett.* **121**, 096401 (2018).
4. Kida, T. et al. The giant anomalous Hall effect in the ferromagnet Fe_3Sn_2 - a frustrated kagome metal. *J. Phys.* **23**, 112205 (2011).
5. Hou, Z. et al. Observation of various and spontaneous magnetic skyrmionic bubbles at room temperature in a frustrated Kagome magnet with uniaxial magnetic anisotropy. *Adv. Mater.* **29**, 1701144 (2017).
6. Altthaler, M. et al. Magnetic and geometric control of spin textures in the itinerant kagome magnet Fe_3Sn_2. *Phys. Rev. Res.* **3**, 043191 (2021).
7. Fenner, L., Dee, A. & Wills, A. Non-collinearity and spin frustration in the itinerant kagome ferromagnet Fe_3Sn_2. *J. Phys.* **21**, 452202 (2009).
8. Trumpy, G., Both, E., Djéga-Mariadassou, C. & Lecocq, P. Mössbauer-effect studies of Iron-Tin alloys. *Phys. Rev. B* **2**, 3477–3490 (1970).
9. Le Caer, G., Malaman, B. & Roques, B. Mossbauer effect study of Fe_3Sn_2. *J. Phys. F* **8**, 323 (1978).
10. Malaman, B., Fruchart, D. & Le Caer, G. Magnetic properties of Fe3Sn2. II. Neutron diffraction study (and Mossbauer effect).*J. Phys. F* **8**, 2389 (1978).
11. Wang, Q., Sun, S., Zhang, X., Pang, F. & Lei, H. Anomalous Hall effect in a ferromagnetic Fe_3Sn_2 single crystal with a geometrically frustrated Fe bilayer kagome lattice. *Phys. Rev. B* **94**, 075135 (2016).
12. Biswas, A. et al. Spin-reorientation-induced band gap in Fe_3Sn_2: optical signatures of Weyl nodes. *Phys. Rev. Lett.* **125**, 076403 (2020).
13. Tanaka, H. et al. Three-dimensional electronic structure in ferromagnetic Fe_3Sn_2 with breathing kagome bilayers. *Phys. Rev. B* **101**, 161114 (2020).
14. Weber, C. P. et al. Similar ultrafast dynamics of several dissimilar Dirac and Weyl semimetals. *J. Appl. Phys.* **122**, 223102 (2017).
15. Marsi, M. Ultrafast electron dynamics in topological materials. *Phys. Status Solidi RRL* **12**, 1800228 (2018).
16. Wu, Q. et al. Quasiparticle dynamics and electron-phonon coupling in Weyl semimetal TaAs. *Phys. Rev. Mater.* **4**, 064201 (2020).
17. Misochko, O. V., Georgiev, N., Dekorsy, T. & Helm, M. Two crossovers in the pseudogap regime of $YBa_2Cu_3O_{7-\delta}$ superconductors observed by ultrafast spectroscopy. *Phys. Rev. Lett.* **89**, 067002 (2002).
18. Ishioka, K., Kitajima, M. & Misochko, O. V. Coherent A_{1g} and E_g phonons of antimony. *J. Appl. Phys.* **103**, 123505 (2008).
19. Schoenlein, R. W., Lin, W. Z., Fujimoto, J. G. & Eesley, G. L. Femtosecond studies of nonequilibrium electronic processes in metals. *Phys. Rev. Lett.* **58**, 1680–1683 (1987).
20. Allen, P. B. Theory of thermal relaxation of electrons in metals. *Phys. Rev. Lett.* **59**, 1460–1463 (1987).
21. Hohlfeld, J. et al. Electron and lattice dynamics following optical excitation of metals. *Chem. Phys.* **87**, 237–258 (2000).
22. Fujimoto, J. G., Liu, J. M., Ippen, E. P. & Bloembergen, N. Femtosecond laser interaction with metallic tungsten and nonequilibrium electron and lattice temperatures. *Phys. Rev. Lett.* **53**, 1837–1840 (1984).
23. Liu, Y. et al. Visualizing electron–phonon and anharmonic phonon–phonon coupling in the kagome ferrimagnet $GdMn_6Sn_6$. *Appl. Phys. Lett.* **122**, 251901 (2023).
24. Wang, Z. X. et al. Unconventional charge density wave and photoinduced lattice symmetry change in the kagome metal CsV_3Sb_5 probed by time-resolved spectroscopy. *Phys. Rev. B* **104**, 165110 (2021).
25. Ratcliff, N., Hallett, L., Ortiz, B. R., Wilson, S. D. & Harter, J. W. Coherent phonon spectroscopy and interlayer modulation of charge density wave order in the kagome metal CsV_3Sb_5. *Phys. Rev. Mater.* **5**, L111801 (2021).
26. Yu, J. et al. All-optical manipulation of charge density waves in kagome metal CsV_3Sb_5. *Phys. Rev. B* **107**, 174303 (2023).
27. Tuniz, M. et al. Dynamics and resilience of the unconventional charge density wave in ScV_6Sn_6 bilayer kagome metal. *Commun. Mater.* **4**, 103 (2023).
28. Elsayed-Ali, H. E., Norris, T. B., Pessot, M. A. & Mourou, G. A. Time-resolved observation of electron-phonon relaxation in copper. *Phys. Rev. Lett.* **58**, 1212–1215 (1987).

29. Wenzel, M. et al. Effect of magnetism and phonons on localized carriers in the ferrimagnetic kagome metals $GdMn_6Sn_6$ and $TbMn_6Sn_6$. *Phys. Rev. B* **106**, L241108 (2022).
30. Wenzel, M. et al. Optical study of RbV_3Sb_5: Multiple density-wave gaps and phonon anomalies. *Phys. Rev. B* **105**, 245123 (2022).
31. Uykur, E. et al. Low-energy optical properties of the nonmagnetic kagome metal CsV_3Sb_5. *Phys. Rev. B* **104**, 045130 (2021).
32. Uykur, E., Ortiz, B. R., Wilson, S. D., Dressel, M. & Tsirlin, A. A. Optical detection of the density-wave instability in the kagome metal KV_3Sb_5. *npj Quantum Mater.* **7**, 16 (2022).
33. Merlin, R. Generating coherent THz phonons with light pulses. *Solid State Commun.* **102**, 207–220 (1997).
34. Ishioka, K., Kitajima, M. & Misochko, O. V. Temperature dependence of coherent A_{1g} and E_g phonons of bismuth. *J. Appl. Phys.* **100**, 093501 (2006).
35. He, B. et al. Coherent optical phonon oscillation and possible electronic softening in WTe_2 crystals. *Sci. Rep.* **6**, 30487 (2016).
36. Cheng, L. et al. Temperature-dependent ultrafast carrier and phonon dynamics of topological insulator $Bi_{1.5}Sb_{0.5}Te_{1.8}Se_{1.2}$. *Appl. Phys. Lett.* **104**, 211906 (2014).
37. Hunsche, S., Wienecke, K., Dekorsy, T. & Kurz, H. Impulsive softening of coherent phonons in tellurium. *Phys. Rev. Lett.* **75**, 1815–1818 (1995).
38. Kamaraju, N., Kumar, S. & Sood, A. K. Temperature-dependent chirped coherent phonon dynamics in Bi_2Te_3 using high-intensity femtosecond laser pulses. *Europhys. Lett.* **92**, 47007 (2010).
39. Tomeljak, A. et al. Dynamics of photoinduced charge-density-wave to metal phase transition in $\mathbf{K}_{0.3}MoO_3$. *Phys. Rev. Lett.* **102**, 066404 (2009).
40. Schäfer, H., Kabanov, V. V., Beyer, M., Biljakovic, K. & Demsar, J. Disentanglement of the electronic and lattice parts of the order parameter in a 1D charge density wave system probed by femtosecond spectroscopy. *Phys. Rev. Lett.* **105**, 066402 (2010).
41. Kim, H. et al. Monoclinic and correlated metal phase in VO_2 as evidence of the Mott transition: coherent phonon analysis. *Phys. Rev. Lett.* **97**, 266401 (2006).
42. Kautzsch, L. et al. Incommensurate charge-stripe correlations in the kagome superconductor $CsV_3Sb_{5-x}Sn_x$. *npj Quantum Mater.* **8**, 37 (2023).
43. Makita, M. et al. Femtosecond phase-transition in hard x-ray excited bismuth. *Sci. Rep.* **9**, 602 (2019).
44. He, G. et al. Phonon anomalies associated with spin reorientation in the Kagome ferromagnet Fe_3Sn_2. *Phys. Status Solidi B* **259**, 2100169 (2022).
45. Balkanski, M., Wallis, R. F. & Haro, E. Anharmonic effects in light scattering due to optical phonons in silicon. *Phys. Rev. B* **28**, 1928–1934 (1983).
46. Misochko, O. V., Hase, M., Ishioka, K. & Kitajima, M. Observation of an amplitude collapse and revival of chirped coherent phonons in bismuth. *Phys. Rev. Lett.* **92**, 197401 (2004).
47. Zeiger, H. J. et al. Theory for displacive excitation of coherent phonons. *Phys. Rev. B* **45**, 768–778 (1992).
48. Stampfli, P. & Bennemann, K. H. Theory for the instability of the diamond structure of Si, Ge, and C induced by a dense electron-hole plasma. *Phys. Rev. B* **42**, 7163–7173 (1990).
49. Jiang, Y. et al. Unconventional chiral charge order in kagome superconductor KV_3Sb_5. *Nat. Mater.* **16**, 1353–1357 (2021).
50. Arachchige, H. W. S. et al. Charge density wave in Kagome lattice intermetallic ScV_6Sn_6. *Phys. Rev. Lett.* **129**, 216402 (2022).
51. Teng, X. et al. Magnetism and charge density wave order in kagome FeGe. *Nat. Phys.* **19**, 814–822 (2023).
52. Blaha, P. et al. *WIEN2k: An Augmented Plane Wave Plus Local Orbitals Program for Calculating Crystal Properties*. (Technischen Universität Wien, Austria, 2019).
53. Blaha, P. et al. WIEN2k: An APW+lo program for calculating the properties of solids. *J. Chem. Phys.* **152**, 074101 (2020).
54. Perdew, J. P., Burke, K. & Ernzerhof, M. Generalized gradient approximation made simple. *Phys. Rev. Lett.* **77**, 3865 (1996).
55. Ambrosch-Draxl, C. & Sofo, J. O. Linear optical properties of solids within the full-potential linearized augmented planewave method. *Comput. Phys. Commun.* **175**, 1–14 (2006).

Acknowledgements

H. C. L. acknowledges support from the National Key R& D Program of China (Grants No. 2016YFA0300504 and No. 2018YFE0202600), and the National Natural Science Foundation of China (Grants No. 11574394, No. 11774423, and No. 11822412). The work in Germany has been supported by the Deutsche Forschungsgemeinschaft (DFG) via Grant UY63/2-1. Computations for this work were done (in part) using the resources of the Leipzig University Computing Center.

Author contributions

M.G.F. and E.U. performed the experiments with technical support from A.P. and S.W. A.A.T., and E.U. performed the DFT calculations. Samples were grown by Q.W. and H.C.L. The paper was written by M.G.F. and E.U. with suggestions from all authors.

Funding

Open Access funding enabled and organized by Projekt DEAL.

Competing interests

The authors declare no competing interests.

Additional information

Supplementary information The online version contains supplementary material available at https://doi.org/10.1038/s41535-024-00642-6.

Correspondence and requests for materials should be addressed to Marcos V. Gonçalves-Faria or Ece Uykur.